https://doi.org/10.22645/udi.2024.6.30.01
도시과학 제13권 제1호 2024. 6 9-16쪽

Tracking nucleation characteristics of calcium aluminate cement powder via dynamic light scattering technique

Kim, Gwang Mok*

Abstract: Nucleation characteristics can greatly affect the evolution of hydrates, and thereby strength development could be affected as well. This study aims to explore the nucleation characteristics of calcium aluminate cement powder. Dynamic light scattering technique was employed to track nuclei of calcium aluminate powder. The independent variable was the reaction periods which varied from 1 minute to 24 hrs. The test results show that a reduction in the particle size until 1 hr of reaction period was observed, which indicated that dissolution of calcium aluminate powder was the dominant reaction within the period. However, a change in the particle size distribution attributable to the nucleation process was also observed within the first 3 minutes of the reaction. an increase in the particle size attributable to the crystal growth was between 1hr and 24 hrs.

Key Words: Nucleation, Calcium aluminate cement, Particle size distribution, Dynamic light scattering

1. Introduction

The invention of calcium aluminate cement (CAC) marked a significant milestone in the history of construction materials. Developed as an alternative to ordinary Portland cement (OPC), CAC emerged in the early 20th century to address specific construction needs that OPC could not meet (Pollmann, 2012). While OPC, made primarily from limestone and clay, offers widespread applicability and cost-effectiveness, CAC distinguishes itself through its unique blend of limestone and bauxite or other alumina sources (Gou et al., 2023).

The clinker composition of CAC is predominantly characterized by calcium aluminates, such as monocalcium aluminate (CA), dicalcium aluminate (C2A) and mayenite (C12A7), which play a crucial role in its hydration reactions (Qi et al., 2020). Upon mixing with water, these calcium aluminates undergo a series of complex reactions that result in the formation of various hydrates, including calcium aluminate hydrates and alumina gel (Ukrainczyk, 2014). This distinct composition endows CAC with rapid hardening and setting properties, making it particularly suitable for time-sensitive and specialized construction projects (Gu et al., 1997).

Extensive research has been conducted to investigate the mechanical performance of CAC (Kirca et al., 2013). Studies have shown that CAC exhibits superior early-age strength compared to OPC, making it an ideal choice for projects demanding rapid load-bearing capacity (Seo et al., 2022; Win et al., 2024). The mechanical properties of CAC, including compressive strength, flexural strength, and fracture toughness, have been thoroughly explored, revealing that CAC-based concretes can achieve remarkable performance (Khaliq et al., 2015). These findings underscore the material's potential for high-stress applications, such as industrial floors, precast structures, and emergency repairs (Khaliq et al., 2015).

In addition to its mechanical performance, the durability of CAC has been a focal point of research. The resistance of the CACs to sulfate attack, high temperatures, and aggressive chemical environments has been widely documented, demonstrating its suitability for use in challenging conditions where OPC might fail (Damion et al., 20

* 한국지질자원연구원 자원활용연구본부 선임연구원, 교신저자 (k.gm@kigam.re.kr).

22; Khaliq et al., 2015). The formation of stable calcium aluminate hydrates and the absence of calcium hydroxide in significant quantities report edly contributed to its enhanced durability (Benst ed, 2002). Moreover, the dense microstructure of CAC-based materials imparts excellent resistance to freeze-thaw cycles and chemical corrosion, fu rther solidifying its role in infrastructure projects requiring longevity and resilience (Adesanya et a l., 2023).

However, nucleation characteristics of the CA C powder have been rarely investigated. The nu cleation characteristics can greatly affect the ev olution of hydrates, and thereby strength develo pment could be affected as well (Vehmas et al., 2017). Thus, studies on the nucleation characteri stics of OPC have been extensively conducted (Vehmas et al., 2017; Scherer et al., 2012; Demo et al., 2012).

This study aims to explore the nucleation char acteristics of CAC powder. Dynamic light scatteri ng (DLS) technique was employed to track nucle i of CAC powder. The independent variable was reaction periods which varied from 1 minute to 24 hrs.

2. Theoretical background

There are three types of particle size analysis techniques often used which are static light scattering, dynamic light scattering method and laser diffraction methods (Krautwurst et al., 2018; Stecher and Plank, 2020; Erdoan et al., 2010). The static light scattering method is classical particle size analysis technique in which particle size is measured under aqueous conditions. The effective detection range of the technique is the micro-sized particles (Ehrl et al., 2006). That is, the sensitivity of the particles with sub-micron in size was relatively weak (Ehrl et al., 2006). Laser diffraction particle size techniques have an intermediate detection range. The technique can detect particles with a size ranging from 10 nm to 3.0 mm (Li et al,. 2019). That is, the technique is applicable to the particles with a wide range of particle size distribution. However, the sensitivity of laser diffraction is lower compared to dynamic light scattering when measuring the particle size distribution of nano-sized particles (Kacker et al., 2018). It is widely known that the particle size of hydrates when the nucleation of cementitious materials is progressed is in the range of approximately tens of nanometers (Schonlein and Plank, 2018; John et al., 2018). Thus, dynamic scattering particle size analysis is widely used for investigating nucleation characteristics of various materials (Tobler et al., 2009; Saridakis et al., 2002; Schubert et al., 2017). The technique is powerful to detect the particles in the range from 1.0 nm to 1.0 μm (Zheng et al., 2016).

3. Experimental Procedure

3.1 Raw materials

The CAC produced by Union Co., Korea was used in the present study, and the chemical composition measured by X-ray fluorescence was shown in Table 1. The Al_2O_3 and CaO components mainly consisted of the CAC used here. The composition of the components was more than 98%. The composition of SiO_2 was 0.14 %. indicating that the CAC might not contain C_2AS phases that are generally observed in CAC powders when Si was sufficiently provided during the manufacturing process of the type of cement (Kim et al., 2023).

Table 1. Chemical composition of CAC

Component	Composition (%)
Al_2O_3	66.8
CaO	32.3
Na_2O	0.36
MgO	0.24
SiO_2	0.14
Fe_2O_3	0.09
SO_3	0.04
P_2O_5	0.04
SrO	0.02
K2O	0.01

Figure 1 shows the XRD patterns of CAC powers. The XRD patterns shows the peaks corresponding to the presence of CA ($CaA_{12}O_4$, ICSD #180997) and CA_2 ($CaAl_4O_7$, ICSD #44519).

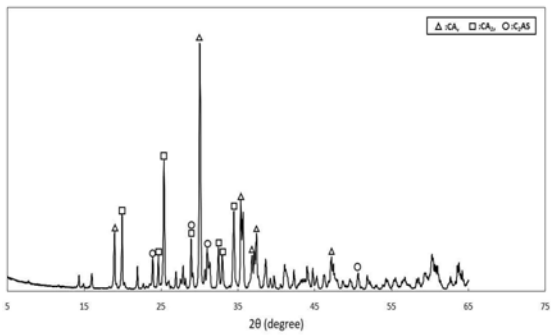

Figure 1. XRD pattern of CAC powder

The corresponding contents of the CA and CA_2 phases in the CAC powder obtained by the Rietveld refinement method were 55.9 and 43.8%, indicating that a small amount of C_2AS was present in the CAC powder.

Figure 2 shows the particle size distribution curves obtained by static light scattering analysis (HELOS). The D10, D50 and D90 values were 1.34 μm, 6.68 μm, and 17.24 μm, respectively. For the formulation of the solution with CAC powders, Ultrapure water (Milli Q, resistivity: 18.2 MΩ · cm) was used and a glass microfiber filter with a pore size of 1.6 m (Whatman, GF/A) was used for the filtration of hydrated powder samples. Anhydrous ethanol (guaranteed reagent grade, OCI Company Ltd.) was employed to prevent unexpected reactions.

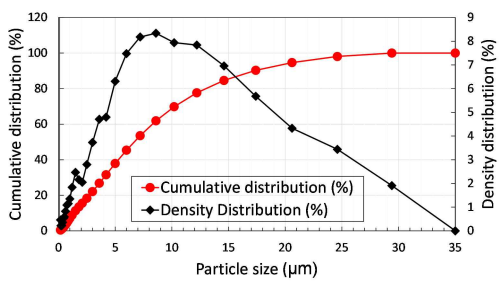

Figure 2. Particle size distribution curves of CAC

3.2 Sample preparation and test methods

The preparation of the solution with CAC po wder was carried out as follows: 10 grams of C AC powders were added to 500 milliliters of ult rapure water, and the mixture was stirred at 30 0 rpm for specified durations. The duration vari ed from 1 minute to 24 hrs. To prevent water evaporation during the reaction period, the solu tion was covered with commercial polyvinyl fil m. The temperature was maintained at 25±1° C throughout the test. At specified intervals, 2. 0 milliliters of the solution were extracted for DLS analysis. The extracted solutions were then mixed with 18.0 milliliters of anhydrous ethanol to halt the hydration reaction and dilute the sol ution. Each DLS test result was conducted with a data acquisition time of 70 seconds.

4. Results and Discussion

Figure 3 shows differential intensity curves of the CAC solution with reaction periods. The differential intensity indicates scattered light intensity across different particle sizes. That is, the type of curve indicates how strongly particles of a specific size scatter light. In the present study, the figure of the differential intensity curve is mostly similar within 3 minutes, while the curve at 30 minutes were different from the curves obtained within 3 minutes. The presence of the particles ranging from several thousand nm was observed in the curve at 30 minutes, which was not detected in the curves within 3 minutes. The particles ranging from 800 nm to 3000 nm and the particles ranging from 20,000 nm to 200,000 nm were only observed in the curves within 3 minutes. Baltakys et al. reported that the first peak in the heat evolution curve of CACs was observed at approximately 10 minutes, indicating that the dissolution of CAC powder and the precipitation of hydrates was initiated around the reaction period (Baltakys et al., 2018). That is, the presence of the particles ranging from several thousand nm in the curve at 30 minutes indicated that the dissolution of the particles

ranging from 20,000 nm to 200,000 nm and the precipitation of hydrates on the surface of the particles ranging from 800 nm to 3000 nm might occurred at the same time between 3 minutes and 30 minutes.

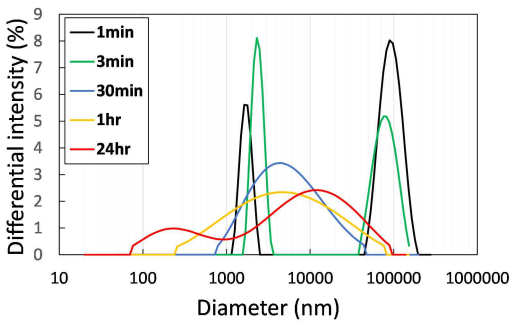

Figure 3. Differential intensity curves of CAC solution with reaction periods

The distribution of the particles in the curves after 30 minutes became wider. The presence of the particles ranging from 100 nm to 500 nm was newly detected in the curve at 1 hr. The presence of the particles ranging from 70 nm to 300 nm was detected in the curve at 24 hrs. Besides, the presence of the particles with a size of more than 30,000 nm was observed in the curves at 1 hr and 24 hrs of reaction period. It has been reported that the second peak in the heat evolution curve of CACs was generally observed at approximately 10 hrs of the reaction period (Baltakys et al. 2018; Puerta-Falla et al., 2015). It can be inferred from the previous studies that a dominant formation of hydrates in CAC solutions possibly occurred between 1hr and 24 hrs (Baltakys et al. 2018; Puerta-Falla et al., 2015). That is, nuclei of hydrates were formed on the surface of CAC powders at the initial reaction within 30 minutes. The hydrates within 30 minutes might partially cover the surface of CAC powders (Jia et al., 2020). The leached reactive components such as Ca and Al ions under these conditions could diffuse more widely into electrolytic solution since the release of reactive ions from CAC powders may slow down (Kim et al., 2023). Furthermore, the concentration of reactive ions may be locally reduced due to the steady consumption of the ions for the formation of hydrates (Embile Jr et al., 1019). These conditions were favorable for the nucleation and observation in the solution with CAC powders at 24 hrs, and thereby the particles ranging from 70 nm to 300 nm were possibly detected in the curve at 24 hrs.

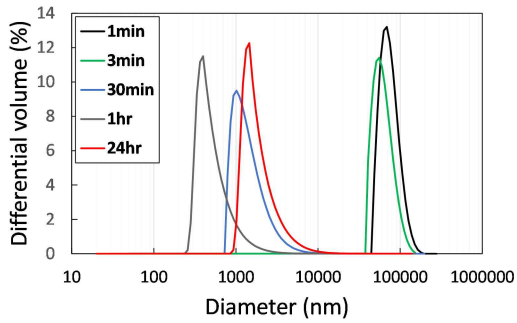

Figure 4. Differential volume curves of CAC solution with reaction periods

Figure 4 shows the differential volume curves of the CAC solution with reaction periods. In general, particle size distribution curves obtained from various particle size analysis techniques are differential volume curves (Jachiet et al., 2018; Hendrix et al., 2019; Erdoan et al., 2010). The differential volume curves in the DLS tests indicate the particle size distribution curves. In the present study, the curves at 1 minute were different from the PSD curve of pristine CAC powder obtained from the SLS test. The particle size obtained from the DLS test at 1 minute was larger than that obtained from the SLS test. It should be noted that the particles with a size of more than 1.0 μm in DLS tests might tend to be overestimated due to the multiple scattering, nonlinear effects, and refraction so on (Farkas and Kramar, 2021). That is, the particles with a size of more than 1.0 μm in the present study were possibly overestimated at 1 minute and 3 minutes, considering for SLS result of pristine CAC powders. Despite the possible

overestimation, a slight reduction of particle size was observed at 3 minutes compared to the particle size at 1 minute, indicating that the dissolution of the CAC during the reaction period was dominant. The particle size of CAC powders in the solution was steadily reduced when the reaction period reached 1 hr, indicating that the dissolution of CAC powders was dominant until 1 hr. In particular, the particles with a size of hundreds of nanometers at 1 hr were observed, which indicated the nucleation actively occurred in the solution. While the particle size increased between 1 hr and 24 hrs. The results were attributable to the growth of hydrates. Generally, more energy is absorbed or released during the crystal growth process compared to the nucleation process (L⌀ge et al., 2023). Therefore, it is assumed that nucleation predominantly occurs at the first peak reported in previous studies, while the second peak, occurring between 1 hour and 24 hours, is attributed to crystal growth.

Figure 5 shows the differential volume curves of CAC solution at 1 minute and 3 minutes in the range from 1,000 nm to 10,000 nm. The differential volume curve in the range at 1 minute was shifted to the left side at 3 minutes. The result indicated an increase in the particle size occurred during the periods. This was possibly induced by the nucleation and precipitation of the nuclei on the surface of CAC particles with a size of approximately 1,000 nm. It can be inferred that the nucleation process in the CAC powders might occur within 3 minutes (Prasittisopin and Sereewatthanawut, 2019; Sereewatthanawut and Prasittisopin, 2022). Furthermore, the initial nucleation occurred around the CAC powder with a size of 1.0 – 2.0 μm.

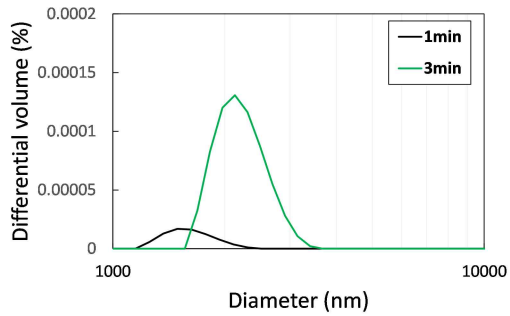

Figure 5. Differential volume curves of CAC solution at 1 minute and 3 minutes in the range from 1,000 nm to 10,000 nm

Overall, nucleation of CAC powders in the solution state was possibly initiated within 3 minutes. However, the dissolution of CAC was the dominant reaction within 1 hr, by which a reduction in the particle size was observed in the DLS test. The growth of hydrates was dominant between 1hr and 24 hrs. The clear shift of the differential volume curve to the right side well supported the reaction characteristics at 24 hrs.

5. Concluding remarks

The nucleation and crystal growth of CAC powders in solutions were investigated using the DLS technique. The main results drawn in the present study are as follows.

(1) The change in the particle size distribution due to the nucleation process was observed within the first 3 minutes of the reaction.

(2) A reduction in the particle size until 1 hr of the reaction period was observed, which indicated that dissolution of CAC powder was the dominant reaction within the period.

(3) An increase in the particle size in the solution with CAC powders at 24 hrs was observed, indicating that the growth of hydrates was the dominant reaction during the period.

The study demonstrated that the nucleation process is rapid and occurs within a few minutes, while crystal growth dominates over a longer period. These findings provide valuable insights into the hydration dynamics of CAC powders, c

ontributing to a better understanding of the nuc leation and growth of hydrates from the CAC p owders.

감사의 글

This work was supported by Korea Institute o f Energy Technology Evaluation and Planning(K ETEP) grant funded by the Korea government (MOTIE)(20212010200080, In-situ carbonation tec hnology development using CO2 emissions from cement industry).

REFERENCES

Baltakys, K., Sarapajevaite, G., & Dambrauskas, T. (2018). The influence of different additiv es on the early-stage hydration of calcium aluminate cement. Journal of Thermal Analy sis and Calorimetry, 134, 89-99.

Bensted, J. (2002). Calcium aluminate cements. Structure and performance of cements, 2, 1 14-138.

Demo, P., Sveshnikov, A., Hokova, Ladman, D., & Ticha, P. (2012). Physical and chemical as pects of the nucleation of cement-based ma terials.

Ehrl, L., Soos, M., & Morbidelli, M. (2006). Sizin g polydisperse dispersions by focused beam reflectance and small angle static light scatt ering. Particle & Particle Systems Characteri zation, 23(6), 438-447.

Embile Jr, R. F., Walder, I. F., & Mahoney, J. J. (2019). Multicomponent reactive transport modeling of effluent chemistry using locally obtained mineral dissolution rates of forsterit e and pyrrhotite from a mine tailings deposi t. Advances in Water Resources, 128, 87-96.

Erdoan, S. T., Nie, X., Stutzman, P. E., & Garb oczi, E. J. (2010). Micrometer-scale 3-D sha pe characterization of eight cements: Particl e shape and cement chemistry, and the effe ct of particle shape on laser diffraction part icle size measurement. Cement and Concret e Research, 40(5), 731-739.

Farkas, N., & Kramar, J. A. (2021). Dynamic lig ht scattering distributions by any means. Jou rnal of Nanoparticle Research, 23(5), 120.

Gou, M., Hou, W., Zhou, L., Zhao, J., & Zhao, M. (2023). Preparation and properties of calc ium aluminate cement with Bayer red mud. Construction and Building Materials, 373, 130 827.

Gu, P., Beaudoin, J. J., Quinn, E. G., & Myers, R. E. (1997). Early strength development an d hydration of ordinary Portland cement/calc ium aluminate cement pastes. Advanced cem ent based materials, 6(2), 53-58.

Hendrix, D., McKeon, J., & Wille, K. (2019). Beh avior of colloidal nanosilica in an ultrahigh p erformance concrete environment using dyn amic light scattering. Materials, 12(12), 1976.

Jachiet, M., Azema, N., Le Saout, G., Garcia-Di az, E., & Kocaba, V. (2018). Influence of tri ethanolamine on cement pastes at early age of hydration. Advances in Cement Research, 30(4), 159-171.

Jia, Z., Chen, C., Zhou, H., & Zhang, Y. (2020). The characteristics and formation mechanism of the dark rim in alkali-activated slag. Cem ent and Concrete Composites, 112, 103682.

John, E., Matschei, T., & Stephan, D. (2018). Nu cleation seeding with calcium silicate hydrat e: A review. Cement and Concrete Researc h, 113, 74-85.

Kacker, R., Maaß, S., Emmerich, J., & Kramer, H. (2018). Application of inline imaging for monitoring crystallization process in a contin uous oscillatory baffled crystallizer. AIChE J ournal, 64(7), 2450-2461.

Khaliq, W., & Khan, H. A. (2015). High tempera ture material properties of calcium aluminat e cement concrete. Construction and Buildin g Materials, 94, 475-487.

Kim, G. M., Park, S. M., & Park, S. W. (2023). Chloride removal of calcium aluminate ceme nts: Reaction and physicochemical characteri stics. Case Studies in Construction Materials, 18, e01975.

Kirca, O., Yaman, I. O., & Tokyay, M. (2013). C ompressive strength development of calcium aluminate cement-GGBFS blends. Cement an d concrete composites, 35(1), 163-170.

Krautwurst, N., Nicoleau, L., Dietzsch, M., Liebe rwirth, I., Labbez, C., Fernandez-Martinez,

A., ... & Tremel, W. (2018). Two-step nucleation process of calcium silicate hydrate, the nanobrick of cement. Chemistry of Materials, 30(9), 2895-2904.

Li, H., Li, J., Bodycomb, J., & Patience, G. S. (2019). Experimental methods in chemical engineering: particle size distribution by laser diffraction-PSD. The Canadian Journal of Chemical Engineering, 97(7), 1974-1981.

Løge, I. A., Anabaraonye, B. U., Bovet, N., & Fosbøl, P. L. (2023). Crystal nucleation and growth: Supersaturation and crystal resilience determine stickability. Crystal Growth & Design, 23(4), 2619-2627.

Pollmann, H. (2012). Calcium aluminate cements-raw materials, differences, hydration and properties. Reviews in Mineralogy and Geochemistry, 74(1), 1-82.

Prasittisopin, L., & Sereewatthanawut, I. (2019). Dissolution, nucleation, and crystal growth mechanism of calcium aluminate cement. Journal of Sustainable Cement-Based Materials, 8(3), 180-197.

Puerta-Falla, G., Kumar, A., Gomez-Zamorano, L., Bauchy, M., Neithalath, N., & Sant, G. (2015). The influence of filler type and surface area on the hydration rates of calcium aluminate cement. Construction and Building Materials, 96, 657-665.

Qi, C., Spagnoli, D., & Fourie, A. (2020). Structural, electronic, and mechanical properties of calcium aluminate cements: Insight from first-principles theory. Construction and Building Materials, 264, 120259.

Saridakis, E., Dierks, K., Moreno, A., Dieckmann, M. W., & Chayen, N. E. (2002). Separating nucleation and growth in protein crystallization using dynamic light scattering. Acta Crystallographica Section D: Biological Crystallography, 58(10), 1597-1600.

Scherer, G. W., Zhang, J., & Thomas, J. J. (2012). Nucleation and growth models for hydration of cement. Cement and Concrete Research, 42(7), 982-993.

Schonlein, M., & Plank, J. (2018). A TEM study on the very early crystallization of CSH in the presence of polycarboxylate superplasticizers: Transformation from initial CSH globules to nanofoils. Cement and Concrete Research, 106, 33-39.

Schubert, R., Meyer, A., Baitan, D., Dierks, K., Perbandt, M., & Betzel, C. (2017). Real-time observation of protein dense liquid cluster evolution during nucleation in protein crystallization. Crystal Growth & Design, 17(3), 954-958.

Seo, J., Nawaz, A., Jang, J. G., & Lee, H. K. (2022). Modifications in hydration kinetics and characteristics of calcium aluminate cement upon blending with calcium sulfoaluminate cement. Construction and Building Materials, 342, 127958.

Sereewatthanawut, I., & Prasittisopin, L. (2022). Effects of accelerating and retarding agents on nucleation and crystal growth of calcium aluminate cement. Open Ceramics, 11, 100290.

Stecher, J., & Plank, J. (2020). Adsorbed layer thickness of polycarboxylate and polyphosphate superplasticizers on polystyrene nanoparticles measured via dynamic light scattering. Journal of colloid and interface science, 562, 204-212.

Tobler, D. J., Shaw, S., & Benning, L. G. (2009). Quantification of initial steps of nucleation and growth of silica nanoparticles: An in-situ SAXS and DLS study. Geochimica et Cosmochimica Acta, 73(18), 5377-5393.

Ukrainczyk, N. (2014). Chemical shrinkage during hydration reactions of calcium aluminate cement. Austin J. Chem. Eng, 1(1).

Vehmas, T., Kronlof, A., & Cwirzen, A. (2017). Effect of additional surfaces on ordinary portland cement early-age hydration. Materials Sciences and Applications, 8(12), 859.

Win, T. T., Prasittisopin, L., Jongvivatsakul, P., & Likitlersuang, S. (2024). Investigating the role of steel and polypropylene fibers for enhancing mechanical properties and microstructural performance in mitigating conversion effects in calcium aluminate cement. Construction and Building Materials, 430, 136515.

Zheng, T., Bott, S., & Huo, Q. (2016). Techniques for accurate sizing of gold nanoparticles using dynamic light scattering with particular application to chemical and biological sensing based on aggregate formation. ACS applied materials & interfaces, 8(33), 21585-21594.